Proton Diffusion in Proton-Conducting Ba2In1.85M0.15O5 (M = In, Ga, Sc, and Y) Investigated with Quasielastic Neutron Scattering

N.B. When citing this work, cite the original published paper.

(article starts on next page)

Article

Proton Diffusion in Proton-Conducting $Ba_2In_{1.85}M_{0.15}O_5$ (M = In, Ga, Sc, and Y) Investigated with Quasielastic Neutron Scattering

Elena Naumovska, Lucas Fine, Adrien Perrichon, Fabio Piccinelli, Niina Jalarvo, Fanni Juranyi, Michael Marek Koza, and Maths Karlsson*

Read Online

ACCESS | Metrics & More | Article Recommendations | Supporting Information

ABSTRACT: Hydrated barium indate oxide, $Ba_2In_2O_5(H_2O)$, is an ideal model system for intermediate-temperature proton-conducting oxides based on the brownmillerite structure. However, fundamental questions surrounding the defect chemistry, proton dynamics, and how they depend on temperature and cation substitution in this material remain to be understood. Here, we investigate the nature of diffusional proton dynamics in $Ba_2In_2O_5(H_2O)_x$ and the cation-substituted materials $Ba_2In_{1.85}M_{0.15}O_5(H_2O)_x$ (M = Ga, Sc, and Y) with $x = 0.70-0.92$, using quasielastic neutron scattering (QENS). Analysis of the QENS data measured upon heating from 22 to 600 K reveals the onset of diffusional proton dynamics at approximately 400 K for the cation-substituted materials, $Ba_2In_{1.85}M_{0.15}O_5(H_2O)_x$ (M = Ga, Sc, and Y), whereas no proton dynamics are observed for the pristine material $Ba_2In_2O_5(H_2O)_x$, in the here probed time-range of 30−300 ps. For temperatures between 400 and 490 K, the proton dynamics can be assigned to a mixture of rotational diffusion of O−H species and proton transfers between neighboring oxygens, with mean residence times in the range of 103−730 ps for both processes, quite independent of M. At the highest measured temperature, 600 K, the observed proton dynamics are of long-range character and can be approximated with a Chudley−Elliott model of jump diffusion with a mean jump length and mean residence time between two successive jumps of approximately 2.5 Å and 0.12 ns, respectively. Our results indicate that substituting indium with trivalent cations, to increase the availability of accessible proton sites along the diffusion pathway, promotes long-range proton diffusion to occur on a faster time scale in cation-substituted barium indate than in the pristine material.

$Ba_2In_{1.85}M_{0.15}O_5(H_2O)_x$ (M = In, Ga, Sc, Y)

$(In,M)O_6$

Proton diffusion

H
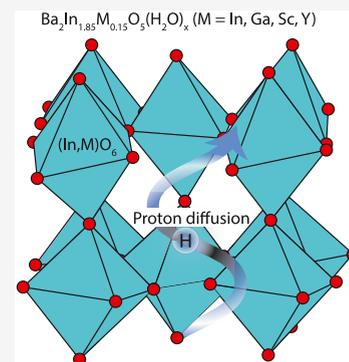
1. INTRODUCTION

Proton-conducting oxides are currently receiving considerable attention because of their promise as electrolytes in future environmentally friendly proton-conducting fuel cells. Barium indate oxide, $Ba_2In_2O_5$, when subjected to a humid atmosphere at elevated temperatures, transforms into the hydrated, proton-conducting oxide $Ba_2In_2O_5(H_2O)_x$, which stands out as an ideal model system for brownmillerite-based proton conductors.[1−5] During the hydration reaction, hydroxyl groups (OH^-) occupy the formerly tetrahedral layers of $Ba_2In_2O_5$ to create a structurally distorted "pseudo-cubic" layer, whereas protons (H^+) are delocalized over the formerly relatively undistorted "cubic" layer (Figure 1). Depending on the hydration conditions, x may take values between 0 (non-hydrated material) and 1 (fully hydrated material). The hydration mechanism is a complex process, which involves a structural phase transition as well as an intermediate phase for $T \geq 300$ °C.[4−8]

Detailed structural studies on the fully hydrated material $Ba_2In_2O_5(H_2O)$ showed that two distinct types of proton sites, H(1) and H(2), are present.[1,8−10] The H(1) protons are covalently bonded to the oxygen atoms that connect the alternating layers of undistorted and distorted InO_6 octahedra and form intraoctahedral hydrogen bonds to neighboring

oxygen atoms.[11] In comparison, the H(2) protons form covalent bonds to oxygen atoms in the heavily distorted octahedral layers and interoctahedral hydrogen bonds to the oxygen atoms of the same layers (Figure 1).[12−14] The different coordination of H(1) and H(2) protons is manifested by significant differences in the degree of hydrogen-bonding between the respective protons and neighboring oxygen.[12] Specifically, the H(1) and H(2) protons are found to exhibit relatively weak and strong hydrogen-bonding, respectively, whereas the amount of H(1) and H(2) protons is virtually the same, indicating half occupancy of the H(1) site and full occupancy of the H(2) site.[12]

With respect to its proton-conducting properties, results from variable temperature QENS and *ab initio* molecular dynamics (AIMD) data showed that the proton-conduction mechanism involves localized motions of the protons, distinguished as rotational diffusion of the O−H(1) species

(a)   Ba$_2$In$_2$O$_5$ (b)   Ba$_2$In$_2$O$_5$(H$_2$O)

□ InO$_4$ ■ InO$_6$ ● O   ● H(1)   ● H(2)   ○ H(3)
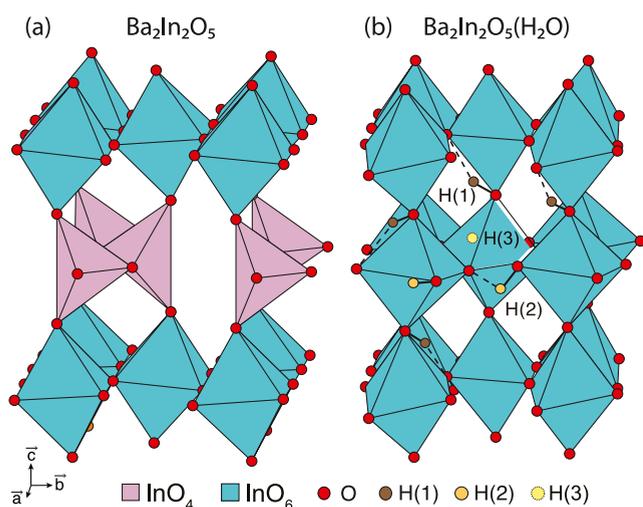
Figure 1. Schematic crystal structures of (a) Ba$_2$In$_2$O$_5$ and (b) Ba$_2$In$_2$O$_5$(H$_2$O). Covalent bonds are represented by continuous black lines, and hydrogen bonds are represented by dashed lines. Ba is not shown in the schematics.

and H(2) proton transfers between neighboring oxygens by investigating samples with two different degrees of hydration, x = 0.30 and 0.92.[14] For x = 0.92, a third proton site was observed, H(3), also included in Figure 1. The H(3) site is found to become occupied upon increasing the temperature and serves as a saddle state for the interexchange between H(1) and H(2) protons.[14] Crucially, the occupation of the H(3) site enables long-range diffusion of protons, which is highly anisotropic in nature and occurs through a two-dimensional pathway.[14] For the less hydrated material (x = 0.30), however, the occupation of the H(3) site and subsequent long-range diffusion are not observed, which is rationalized by hindered dynamics of H(2) protons in the vicinity of oxygen vacancies.[14] Various cation substitutions on the In sites, Ba$_2$In$_{1.85}$M$_{0.15}$O$_5$(H$_2$O)$_x$ with M = In, Ga, Sc, and Y, have also been investigated and showed an increase in the population of the H(1) site upon the substitution of In with any of the three different cations M = Ga, Sc, and Y, with the strongest effect seen for M = Ga and Sc.[13] Interestingly, the cation substitution has been shown to lead to a general increase of the proton conductivity of the material,[15] which suggests that the proton conductivity may be directly linked to the relative occupation of the two types of proton sites, H(1) and H(2).

In this work, we investigate the nature of the localized diffusional proton dynamics in Ba$_2$In$_{1.85}$M$_{0.15}$O$_5$(H$_2$O)$_x$ with M = In, Ga, Sc, and Y, using QENS. The aim of the study is to unravel the effect of cation substitution on the localized and long-range (translational) proton dynamics.

2. EXPERIMENT

2.1. Synthesis and Characterization of Powder Samples. Powder samples of Ba$_2$In$_{1.85}$M$_{0.15}$O$_5$ with M = In, Ga, Sc, and Y were prepared by solid-state synthesis by mixing stoichiometric amounts of the starting reagents BaCO$_3$, In$_2$O$_3$, and M$_2$O$_3$ (M = In, Ga, Sc, or Y). The sintering process was divided into three repetitive heat treatments at T = 1000 °C for 8 h, T = 1200 °C for 72 h, and at T = 1325 °C for 48 h, with intermediate cooling, grinding, and compacting of pellets between each sintering step. The phase purity of the as-prepared samples was confirmed by powder X-ray diffraction (PXRD), see Figure S1 in the Supporting Information (SI). Hydrated samples were prepared by annealing a portion of the as-prepared powders in a tube furnace subjected to a nitrogen flow with water vapor, while cooling from 500 to 200 °C at a rate of 0.1 °C/min. The hydrated samples, Ba$_2$In$_{1.85}$M$_{0.15}$O$_5$(H$_2$O)$_x$ with M = In, Ga, Sc, and Y, are referred to as BIO, Ga/BIO, Sc/BIO, and Y/BIO, respectively. Thermal gravimetric analysis (TGA) of a portion of the hydrated samples established their degree of hydration, x, to 70% (BIO), 77% (Ga/BIO), 78% (Sc/BIO), and 92% (Y/BIO) (Figure S2). Furthermore, infrared (IR) absorbance spectroscopy measurements were performed on all samples and compared with the literature on the same materials in order to check for reproducibility and confirm the local coordination of protons in each material (Figures S3−S5).

2.2. Quasielastic Neutron Scattering. The QENS measurements were performed on the near-backscattering, crystal-analyzer spectrometer BASIS at the Spallation Neutron Source at the Oak Ridge National Laboratory in the U.S.[16] The measurements were performed using the Si(111) analyzer crystal, for which the instrument features an energy resolution of 3.5 μeV at full width at half-maximum (fwhm) of the elastic line, an energy transfer (E) range of −100 to 100 μeV, and a momentum transfer (Q) range of 0.2−2.0 Å^{-1}. Measurements were taken at the temperatures T = 22, 400, 450, 490 K for Ga/BIO, T = 22, 400, 490, 600 K for Sc/BIO, T = 22, 400, 450, 490, 600 K for Y/BIO and T = 22, 400, 490, 600 K for BIO. The 22 K data was used as a resolution function in the data analysis. Measurements were also performed on a vanadium standard and on an empty sample container (both at 300 K) to correct for the efficiency of different detectors and the background contributions from the sample container and the sample environment. In the data evaluation, the measured scattering intensity, $S(Q, E)_{meas}$, was fitted to the following function

$$S(Q, E)_{meas} = S(Q, E) \otimes R(Q, E) + bkg(Q) \tag{1}$$

where

$$S(Q, E) = I_D(Q)\delta(E) + I_L(Q)L(Q, E) \tag{2}$$

Here, $S(Q, E)$ is the dynamical structure factor, $R(Q, E)$ is the instrumental resolution function, bkg contains contributions from residual instrumental background as well as from inelastic scattering events (phonons), $I_D(Q)$ multiplied with a Dirac delta function $\delta(E)$ represents the elastic scattering, and $I_L(Q)$ multiplied with a Lorentzian function $L(Q, E)$ describes the quasielastic scattering. The data reduction and analysis were performed using the Mantid software.[17] QENS measurements were also taken on the time-of-flight (TOF) spectrometer FOCUS at the Paul-Scherrer Institute in Switzerland, but these data did not show any significant QENS signal for any of the samples (see the SI).

3. RESULTS

3.1. Dynamical Structure Factors. Measurements of the dynamical structure factor, $S(Q, E)_{meas}$, of the pristine compound, BIO, did not show a significant quasielastic scattering signal for any of the probed temperatures (T = 400, 490, and 600 K), see Figure S6 for the 600 K data. Therefore, these spectra were not further analyzed. For the doped materials, M/BIO (M = Ga, Y, and Sc), measurements

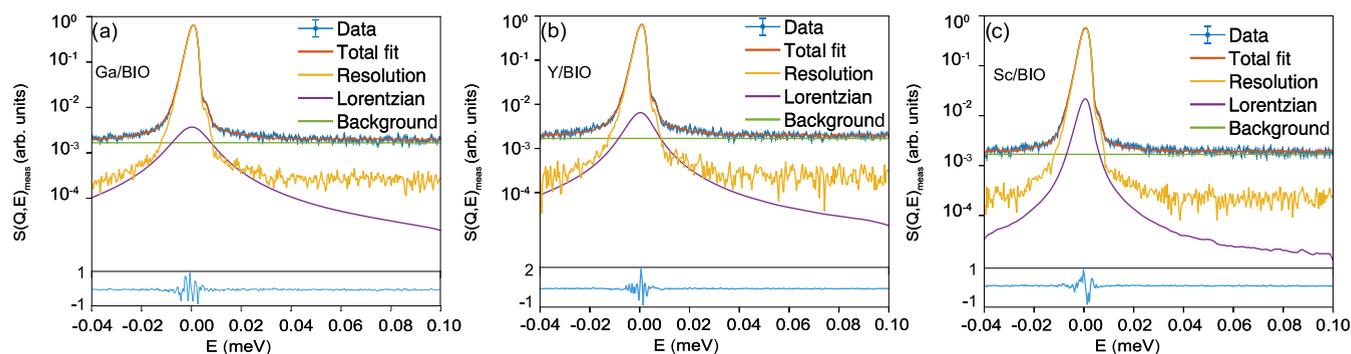**Figure 2.** $S(Q, E)_{meas}$ at $Q = 1.50$ Å^{-1} together with fits measured with the Si(111) analyzer at $T = 490$ K for (a) Ga/BIO, (b) Y/BIO, and (c) Sc/BIO.

of $S(Q, E)_{meas}$ revealed significant quasielastic scattering for $T \geq 400$ K. Figure 2 shows the $S(Q, E)_{meas}$ for the three materials at $T = 490$ K and $Q = 1.50$ Å^{-1}, together with fits to eqs 1 and 2; data for additional temperatures and Q values are shown in Figures S7−10. Our fitting analysis shows that the spectra can be adequately fitted to a single Lorentzian function. Interestingly, the Q-dependence of the line width (Γ) of the Lorentzian fwhm, which can give information about the spatial restriction of the dynamics, was found to vary with temperature, as shown in Figure S11. Up to $T = 490$ K, Γ does not (within error) depend significantly on Q (Figure S11), for any of the three materials, whereas for $T = 600$ K, Γ increases with increasing Q. Within the probed energy window and the energy resolution of the instrument, our observations suggest that below $T = 490$ K, the observed dynamics are mainly localized in nature, whereas at $T = 600$ K, it is long-range in nature. Mechanistic details, such as the mean relaxation time τ and spatial geometry of each dynamics process, are analyzed in the following.

3.2. Localized Proton Dynamics. The mean relaxation time of the localized dynamics can be derived from the quasielastic line width as $\tau = 2\hbar/\overline{\Gamma}$, where $\overline{\Gamma}$ is the Q-averaged value of Γ. τ takes values in the range of 103−210(10) ps for Ga/BIO, 124−156(10) ps for Y/BIO, and 700−731(90) ps for Sc/BIO. The relatively high value and large error obtained for Sc/BIO exceed the instrument resolution and should therefore be interpreted cautiously. This result stems from the particularly weak quasielastic signal detected for this material, which impedes a robust data analysis.

The mean relaxation time of ca. 100−200 ps (Sc/BIO excluded) does not differ significantly among the different materials and is considerably longer than what has previously been measured for the proton transfer and O−H rotational diffusion (<30 ps) for both brownmillerite and perovskite-based proton-conducting oxides.[14,18−21] However, in the previous AIMD and QENS study of BIO, it was found that the H(3) site, which becomes occupied upon increasing temperature and that serves as a saddle state for the interexchange between H(1) and H(2) protons and hence enables long-range proton diffusion, is characterized by a mean relaxation time of 77 ps related to localized dynamics.[14] This timescale is quite similar to the timescale of the localized dynamics as observed in our study, which may indicate that the localized dynamics as observed here involve the H(3) site.

Information about the spatial geometry of the localized proton dynamics, as observed for $T = 400$, 450, and 490 K, can be obtained from the analysis of the elastic incoherent

structure factor (EISF), which is defined as the ratio of the elastic amplitude over the sum of the elastic and quasielastic amplitudes, i.e., EISF $= I_D/(I_D + I_L)$. Figure 3 shows the EISF for Ga/BIO, Y/BIO, and Sc/BIO together with fits to a jump-diffusion model over two ($N = 2$) and four ($N = 4$) equivalent sites. These models are widely used for describing, respectively, the proton transfer and O−H rotational motion in proton-conducting oxides.[14,18,20−23] Note, a constant c has been added to the respective EISF model functions in order to take into account elastic scattering due to *immobile* protons, that is, protons undergoing dynamics that are too slow to be resolved by the instrument (see S4.3 for details). As can be seen from Figure 3, both models equally well describe the experimental EISFs in the probed Q-range, for all three materials. The fitted parameter, i.e., the jump length, takes values in the range of $d_{2N} = 1.86$−2.76 Å ($N = 2$ model) and $r_{4N} = 1.09$−1.70 Å ($N = 4$ model), see Table 1. We note that the jump length for the $N = 2$ model is longer than the calculated values as obtained for the H(1) protons ($d_{2N} = 1.6$−1.9 Å) and H(2) protons ($d_{2N} = 0.6$−0.8 Å).[12,14] Further, the jump length for the $N = 4$ model, which shall be compared to the O−H bond length, is longer than the expected value of (0.97−1.02 Å).[12,14]

Additional fitting analysis on our EISF data for $T = 400$ K was performed by fixing jump lengths to the calculated values at 300 K from ref 14, corresponding to $d_{O−H(1)} = 1.6$ Å and $d_{O−H(2)} = 0.6$ Å (Figure S12). As can be seen, the EISF equally well describes both jump distances, implying that our data cannot be simply assigned to the H(1) or H(2) sites, nor to the two dynamical processes ($N = 2$ or 4). Instead, the results point toward the QENS signal being more complex in nature and may be due to both proton transfer and O−H rotational processes. The interpretation of the QENS data in terms of such complex dynamics implies that the mean relaxation time τ of the localized dynamics corresponds to an average of the mean relaxation times for the different proton motions. This is in agreement with previous QENS studies on similar proton-conducting oxides, such as hydrated BaZr$_{1−x}$In$_x$O$_{3−x/2}$ ($x = 0.10$ and 0.20)[18,19] and BaZr$_{1−x}$Sc$_x$O$_{3−x/2}$ ($x = 0.10$ and 0.50).[21] To distinguish between the two types of dynamics, one would need to explore a larger Q-range, up to, at least 4 Å^{-1}, which is also in agreement with these previous studies.[18,19,21]

The fraction of immobile protons, c, takes values in the range of 93−96% for Ga/BIO, 93−96% for Y/BIO, and 89−93% for Sc/BIO (Table 1), which thus suggests that the major part of the protons scatter elastically with respect to the instrument resolution. The immobile fractions of the doped
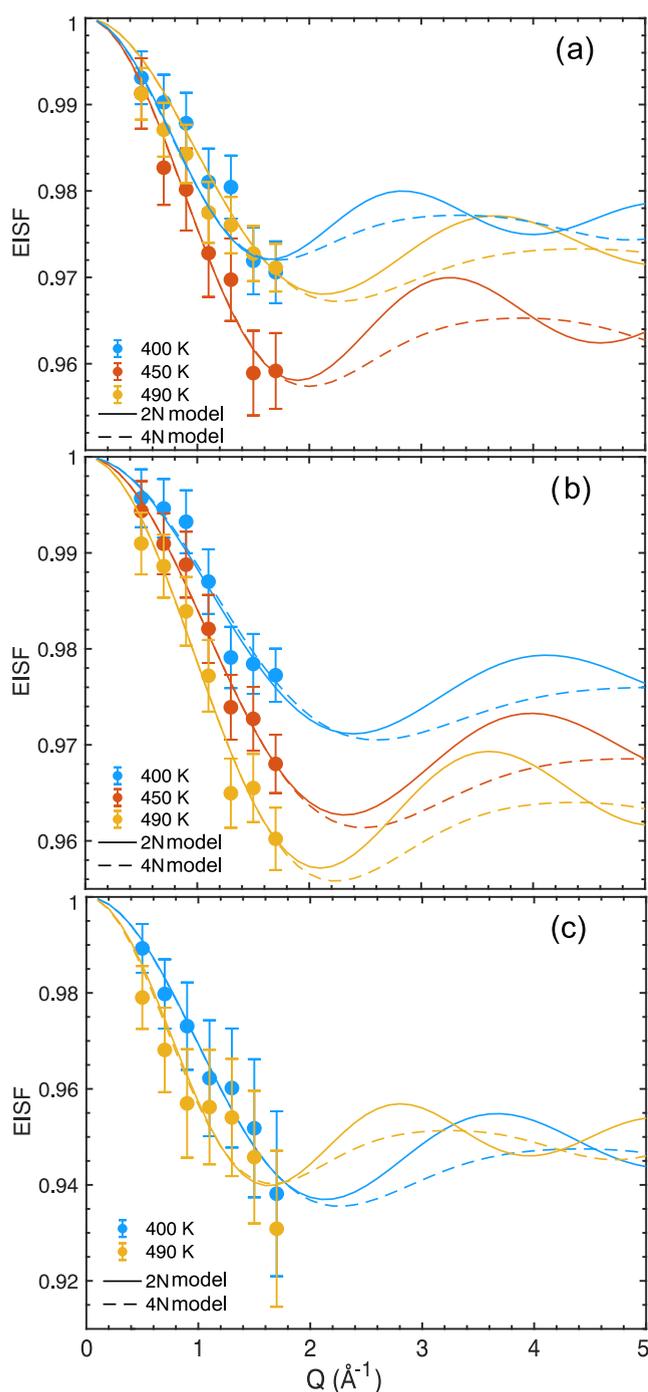
Figure 3. EISFs for (a) Ga/BIO, (b) Y/BIO, and (c) Sc/BIO, as derived from the BASIS data. The lines are free fits to the jump-diffusion model over two ($N = 2$) and four ($N = 4$) sites.

Table 1. Compilation of Parameters for the EISF Analysis (Figure 3)[a] and the Analysis with the C−E Model (Figure 4)[b,c]

model	T (K)	400	450	490	600
$N = 2$	r_{2N} (Å)	1.05(27)	1.18(21)	1.36(18)	
	c_{2N}(%)	95(3)	93(2)	95(1)	
	R^2	0.956	0.960	0.957	
$N = 4$	r_{4N} (Å)	1.25(40)	1.42(32)	1.65(23)	
	c_{4N} (%)	96(1)	95(1)	96(1)	
	R^2	0.948	0.953	0.968	
Y/BIO					
$N = 2$	r_{2N} (Å)	0.93(50)	0.97(14)	1.07(30)	
	c_{2N} (%)	95(4)	94(3)	93(3)	
	R^2	0.880	0.974	0.955	
$N = 4$	r_{4N} (Å)	1.09(60)	1.14(33)	1.27(38)	
	c_{4N} (%)	96(3)	95(2)	94(2)	
	R^2	0.924	0.974	0.962	
C−E	d_{C-E} (Å)				2.52(80)
	τ_{C-E} (ps)				122(37)
	R^2				0.917
Sc/BIO					
$N = 2$	r_{2N} (Å)	1.05(30)		1.38(42)	
	c_{2N} (%)	89(3)		90(2)	
	R^2	0.960		0.764	
$N = 4$	r_{4N} (Å)	1.26(42)		1.70(57)	
	c_{4N} (%)	93(3)		93(2)	
	R^2	0.743		0.954	
C−E	d_{C-E} (Å)				2.64(70)
	τ_{C-E} (ps)				117(28)
	R^2				0.849

[a]Jump-diffusion model of N equivalent sites placed upon a circle of radius r. For $N = 2$, the jump distance is $d = 2r$; for $N = 4$, it is $d = r\sqrt{2}$. [b]The C−E model assumes $\Gamma(Q) = 2\hbar/\tau[1 - (\sin(Qd))/Qd]$. [c]The R-square values (R^2) indicate the goodness of the fit.

dynamics in BIO-based materials than in their cubic counterparts. The large fraction of immobile protons would then be rationalized as protons experiencing dynamics that are simply too slow with respect to the time scale accessed by the instrument.

Alternatively, the large values of c could also be explained if a population of protons is unable to participate in diffusion processes, which can be inferred by the lack of temperature dependency of c and the overall lower intensity of the QENS signal in BIO-based materials than in their cubic counterparts, despite their higher proton concentration. Indeed, hydrated BIO features strongly bonded protons, not found in cubic proton-conducting perovskites, which are present not only at room temperature but are also stable up to ca. 400 °C,[8,10] and persist well beyond the onset of dehydration and up to 700 °C. This is evidenced in the TGA results (Figure S2) with BIO showing a small gradual dehydration in the range of 400−700 °C, followed by a significant and rapid mass loss at 700 °C. The presence and persistence in temperature of these strongly bonded "structural" protons are less pronounced in the M-doped materials, as evidenced in the TGA results (Figure S2) by the lower onset of dehydration of ca. 300 °C for Ga/BIO, Y/BIO, and Sc/BIO. Note, however, that the onset of dehydration in M/BIO is significantly higher than in cubic-structured perovskite materials, typically ca. 200 °C,[24−25][26] which suggests that a population of strongly bonded protons is also present in the doped M/BIO materials.

materials are, within error, constant with temperature and have no clear dependence on the nature of the dopant atom. The values are similar to those reported in a previous QENS study on hydrated $Ba_2In_2O_5$, with immobile fractions of $c = 90(3)$ to $82(2)\%$ for the temperature range between 400 and 485 K.[14] In comparison, smaller values of c have been reported in cubic-structured proton-conducting perovskites, in the range, for instance, of 50−60% for Y- and Sc-doped $BaZrO_3$.[18,20,21,24] This trend of a higher fraction of immobile protons in hydrated brownmillerite-structured materials than in cubic-structured perovskite materials could be related to overall slower proton

3.3. Long-Range Proton Dynamics. Figure 4 shows $\Gamma(Q)$ at T = 600 K for (a) Y/BIO and (b) Sc/BIO. Included in
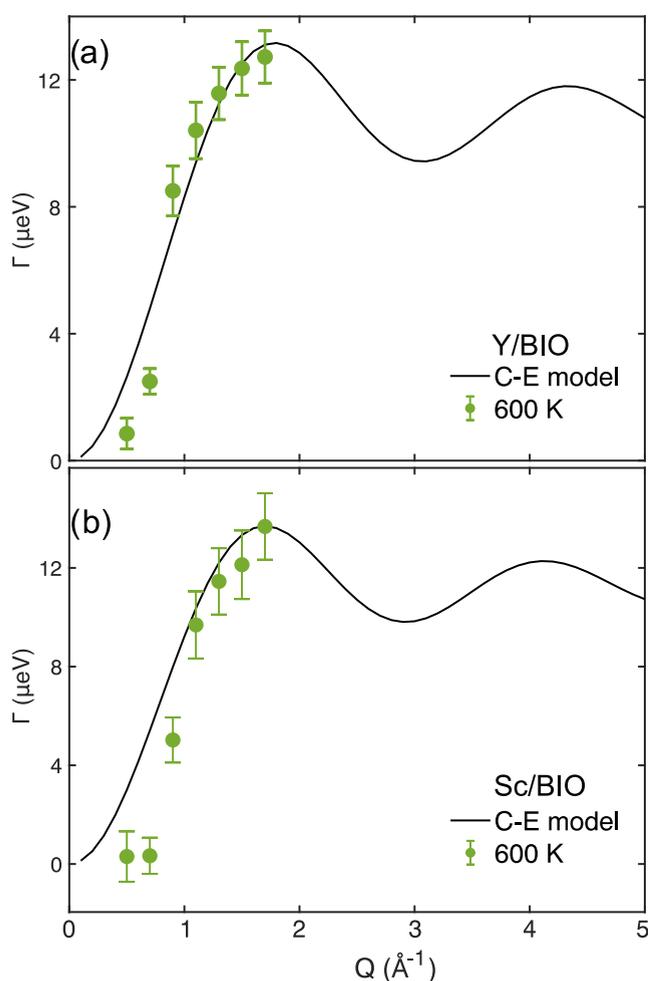

Figure 4. Q-dependence of the fwhm (Γ) at T = 600 K for (a) Y/BIO and (b) Sc/BIO. The lines are fits to the C−E jump diffusion model.

the graphs are fits to a Chudley−Elliott (C−E) model of jump diffusion, which describes long-range diffusion as a series of jumps with a fixed jump length d_{C-E} and a mean residence (relaxation) time τ_{C-E}.[27] For both materials, a free fit of the C−E model to the data yields a reasonable fit; the small misfit for Q < 1 Å^{-1} is considered less important because of the weaker QENS signal in this Q-range. It must be understood that due to the limited Q-range, it is not possible to conclusively determine the correct diffusion model.

For Y/BIO, the obtained jump distance and mean residence time are d_{C-E} = 2.52(80) Å and 122(37) ps. For Sc/BIO, the respective values are d_{C-E} = 2.64(70) Å and 117(28) ps. Note that, for both materials, d_{C-E} is comparable to the fitted localized proton transfer jump length (cf. Section 3.2 and Table 1), exactly as expected for a long-range diffusion mechanism involving individual proton transfer events. Moreover, for Y/BIO, the mean residence time closely matches that of localized proton dynamics ([122(37)] ps for long-range and 124−156(10) ps for localized proton dynamics), suggesting that between 490 and 600 K, the dynamics in this material gradually shift to long-range motion within the probed time window of 30−300 ps, whereas the localized dynamics becomes too fast to be observed within the time window. In

contrast, for Sc/BIO, the mean residence time is found to be significantly shorter than that of localized proton dynamics (117(28) ps for long-range and 700−731(90) ps for localized proton dynamics). However, one should note that the obtained Γ values for Sc/BIO below 600 K are close to the instrumental resolution, which thus indicates a large uncertainty in the obtained time scales for localized proton dynamics in Sc/BIO. Notably, the mean residence times for the long-range jump-diffusion mechanism for Y/BIO (122(37) ps) and Sc/BIO (117(28) ps) are considerably smaller than the ones reported in the previous QENS studies of BIO (≈0.5−6.6 ns).[14]

4. DISCUSSION

By bringing together the results of the analyses of the QENS data, we can now understand several new features pertaining to proton dynamics in BIO and in the cation-substituted equivalents Ga/BIO, Y/BIO, and Sc/BIO. An important, unexpected observation is the absence of a clear QENS signal for BIO. At first glance, this finding contrasts with previous QENS measurements of BIO, which showed a significant QENS signal at similar measuring temperatures.[12,14] This discrepancy likely stems from differences in instrumentation. The TOFTOF spectrometer used in the previous studies[14,28] featured an energy resolution of 480 μeV, which limits the study to dynamics with a characteristic relaxation time faster than a few picoseconds. At these time scales, only the dynamical signatures of H(1) and H(2) could be identified. The signature of H(3) in ref 14 was detected at the limit of the dynamical range of the IN16B spectrometer, a backscattering instrument with a resolution of 0.75 μeV, which also allowed for observing long-range translational diffusion. In comparison, the BASIS instrument used in this study has an energy resolution of 3.5 μeV, which allows measurements of dynamics as slow as some hundreds of picoseconds. This is well suited to cover the dynamical signature of H(3) but may not capture the faster dynamics of H(1) and H(2), nor the slower translational dynamics. As a result, the two sets of data are not directly comparable, as they probe different time scales and hence, potentially, different dynamics. Regarding the absence of the H(3) QENS signature in BIO in the present study, it may be due to a combined effect from the intrinsically weak QENS signal in BIO, the neutron absorbing nature of the sample due to the large neutron absorption cross section of indium, and to difference in sample geometry as thin samples in annular cells were used in the present study, while thick samples in flat cells were used in ref 14. Nevertheless, our results imply that the time scale of the proton dynamics is markedly different between the nonsubstituted and cation-substituted materials, as only the cation-substituted ones exhibit proton dynamics within the here probed time range of 30−300 ps. Our results thus indicate that the strategy of substituting indium with other trivalent cations may be an effective way to promote long-range proton diffusion on a faster time scale than in BIO.

Interestingly, there seems to be no clear, direct correlation between the nature of the substituting cations and the proton dynamics as seen by QENS. There also seems to be no correlation between the proton dynamics and the degree of hydration (77−92%), nor with the crystal structure and cell parameters (see the SI). To shed further light on this, we investigated the local coordination environments of the protons by performing a peak fit analysis of the IR spectra of all materials (see the SI). Our results from this analysis show

that the local proton environments are comparable between the pure and cation-substituted materials, with no significant difference in terms of, e.g., hydrogen-bond strength, which is in full agreement with a previous report.[12] Regarding the relative distribution of protons between the H(1) and H(2) sites, which can qualitatively be approximated from the integrated intensities of the IR absorption bands, we found a comparable ratio of the H(1) and H(2) signatures for Ga/BIO and Sc/BIO, whereas the contribution of H(1) sites is relatively smaller for BIO and Y/BIO, also in agreement with ref 13. Thus, there also seems to be no clear correlation between the H(1)/H(2) ratio and the nature and rate of the localized proton dynamics in the cation-substituted materials, which is consistent with the similar local proton environments present in these materials.

As the difference in proton dynamics as seen by QENS between pristine and cation-substituted BIO cannot be simply explained by the nature of the dopant, the hydration level, the average structure, the local environments and distribution of the protons in the materials, nor the geometry of the elementary diffusion motions, we speculate that the difference in dynamics may be due to the H(3) site availability. Indeed, the two-dimensional diffusion pathway proposed for BIO relies on the interexchange between the H(1) and H(2) sites, through the intermediate H(3) sites.[13] To complete a long-range diffusion event, this mechanism relies on two consecutive localized diffusion motions. First, a proton from the H(1) or H(2) site has to diffuse to the H(3) site, then this H(3) proton has to further diffuse to a neighboring vacant H(2) or H(1) site. The large proton content—and thus the lack of vacant sites, leading to a saturation of the diffusion pathway in BIO—has been discussed as a factor that limits the proton diffusivity in this material.[9,13]

The significantly shorter residence time for the long-range diffusion process as found by QENS in the cation-substituted materials, with respect to BIO, may thus indicate that the saturation of the proton path is lessened or that the energy barrier for a proton to diffuse to the H(3) site is lowered due to the substitution of indium by trivalent cations. This raises questions, such as whether there is an optimal level of cation substitution for maximizing the proton diffusivity, and whether cations of different charge will behave in the same way. These questions may stimulate further studies in this field.

5. CONCLUSIONS

Our variable temperature QENS study on $Ba_2In_2O_5(H_2O)_x$ and the cation-substituted materials $Ba_2In_{1.85}M_{0.15}O_5(H_2O)_x$ (M = Ga, Sc and Y) with $x = 0.70-0.92$ reveals the transition from localized proton dynamics between 400 and 490 K, to long-range proton dynamics at 600 K for the cation-substituted materials, whereas we observe no proton dynamics for $Ba_2In_2O_5(H_2O)_x$, in the here probed time-range of 30−300 ps. Detailed analysis of the Q-dependence of the intensity and line width of the quasielastic scattering suggests that the localized proton dynamics are related to a mixture of rotational diffusion of O−H species and proton transfers between neighboring oxygens, with mean residence times in the range of 103−730 ps for both processes, quite independent of M. Furthermore, the long-range proton dynamics can be adequately modeled by a Chudley−Elliott model of jump diffusion, with a mean jump length and mean residence time between two successive jumps of approximately 2.5 Å and 0.12 ns, respectively, also quite independent of M. It follows that,

while the cation substitution is shown to lead to faster localized and long-range proton dynamics, the type of substituting cation appears to have a minor role in the nature (i.e., time scale and spatial geometry) of the dynamics. Our results instead indicate that the beneficial effect of trivalent-cation substitution of BIO is related to an increased availability of the H(3) proton site that enables long-range diffusion on a faster time scale.

◾ ASSOCIATED CONTENT

ⓢ Supporting Information

The Supporting Information is available free of charge at https://pubs.acs.org/doi/10.1021/acs.jpcc.5c04230.

> Details on the PXRD data with Rietveld analysis; thermogravimetric data and analysis; IR spectroscopy data and analysis; and QENS, additional data and analysis (PDF)

◾ AUTHOR INFORMATION

Corresponding Author

Maths Karlsson − *Department of Chemistry and Chemical Engineering, Chalmers University of Technology, SE-412 96 Göteborg, Sweden;* ⓞ orcid.org/0000-0002-2914-6332; Email: maths.karlsson@chalmers.se

Authors

Elena Naumovska − *Department of Chemistry and Chemical Engineering, Chalmers University of Technology, SE-412 96 Göteborg, Sweden;* ⓞ orcid.org/0000-0001-6011-5369

Lucas Fine − *Department of Chemistry and Chemical Engineering, Chalmers University of Technology, SE-412 96 Göteborg, Sweden; Institut Laue Langevin, 38042 Grenoble, France;* ⓞ orcid.org/0000-0003-2755-1980

Adrien Perrichon − *European Spallation Source, SE-221 00 Lund, Sweden;* ⓞ orcid.org/0000-0003-0520-0469

Fabio Piccinelli − *Luminescent Materials Laboratory, Dipartimento di Biotecnologie, University of Verona and INSTM, UdR Verona, 37134 Verona, Italy;* ⓞ orcid.org/0000-0003-0349-1960

Niina Jalarvo − *Neutron Scattering Division, Oak Ridge National Laboratory, Oak Ridge,, Tennessee 37831-6473, United States;* ⓞ orcid.org/0000-0003-0644-6866

Fanni Juranyi − *PSI Center for Neutron and Muon Sciences, Villigen CH-5232, Switzerland;* ⓞ orcid.org/0000-0002-3223-072X

Michael Marek Koza − *Institut Laue Langevin, 38042 Grenoble, France;* ⓞ orcid.org/0000-0002-5133-8584

Complete contact information is available at: https://pubs.acs.org/10.1021/acs.jpcc.5c04230

Notes

The authors declare no competing financial interest.

◾ ACKNOWLEDGMENTS

■ REFERENCES

(1) Jayaraman, V.; Magrez, A.; Caldes, M.; Joubert, O.; Taulelle, F.; Rodriguez-Carvajal, J.; Piffard, Y.; Brohan, L. Characterization of perovskite systems derived from $Ba_2In_2O_5$: Part I: The oxygen-deficient $Ba_2In_{2(1−x)}Ti_{2x}O_{5+x}\square_{1−x}$ ($0 \le x \le 1$) compounds. *Solid State Ionics* **2004**, *170*, 25.

(2) Speakman, S. A.; Richardson, B. J.; Mitchell, B. J.; Misture, S. T. In-situ diffraction study of $Ba_2In_2O_5$. *Solid State Ionics* **2002**, *149*, 247.

(3) Berastegui, P.; Hull, S.; García-García, F. J.; Eriksson, S. G. The Crystal Structures, Microstructure and Ionic Conductivity of $Ba_2In_2O_5$ and $Ba(In_xZr_{1−x})O_{3−x/2}$. *J. Solid State Chem.* **2002**, *164*, 119−130.

(4) Fischer, W.; Reck, G.; Schober, T. Structural transformation of the oxygen and proton conductor $Ba_2In_2O_5$ in humid air: an in-situ X-ray powder diffraction study. *Solid State Ionics* **1999**, *116*, 210−215.

(5) Schober, T.; Friedrich, J.; Krug, F. Phase transition in the oxygen and proton conductor $Ba_2In_2O_5$ in humid atmospheres below 300 °C. *Solid State Ionics* **1997**, *99*, 9−13.

(6) Schober, T.; Friedrich, J. The oxygen and proton conductor $Ba_2In_2O_5$: Thermogravimetry of proton uptake. *Solid State Ionics* **1998**, *113−115*, 369−375.

(7) Islam, M. S.; Davies, R. A.; Fisher, C. A. J.; Chadwick, A. V. Defects and protons in the $CaZrO_3$ perovskite and $Ba_2In_2O_5$ brownmillerite: computer modelling and EXAFS studies. *Solid State Ionics* **2001**, *145*, 333.

(8) Bielecki, J.; Parker, S. F.; Mazzei, L.; Börjesson, L.; Karlsson, M. Structure and dehydration mechanism of the proton conducting oxide $Ba_2In_2O_5(H_2O)_x$. *J. Mater. Chem. A* **2016**, *4*, 1224−1232.

(9) Bielecki, J.; Parker, S. F.; Ekanayake, D.; Rahman, S. M. H.; Börjesson, L.; Karlsson, M. Short-range structure of the brownmillerite-type oxide $Ba_2In_2O_5$ and its hydrated proton-conducting form $BaInO_3H$. *J. Mater. Chem. A* **2014**, *2*, 16915−16924.

(10) Martinez, J.-R.; Mohn, C. E.; Stølen, S.; Allan, N. L. $Ba_2In_2O_4(OH)_2$: Proton sites, disorder and vibrational properties. *J. Solid State Chem.* **2007**, *180*, 3388−3392.

(11) Dervişoğlu, R.; Middlemiss, D. S.; Blanc, F.; Lee, Y.-L.; Morgan, D.; Grey, C. P. Joint Experimental and Computational ^{17}O and ^1H Solid State NMR Study of $Ba_2In_2O_4(OH)_2$ Structure and Dynamics. *Chem. Mater.* **2015**, *27*, 3861−3873.

(12) Perrichon, A.; Jiménez-Ruiz, M.; Mazzei, L.; Rahman, S. M. H.; Karlsson, M. Local structure and vibrational dynamics of proton conducting $Ba_2In_2O_5(H_2O)_x$. *J. Mater. Chem. A* **2019**, *7*, 17626−17636.

(13) Mazzei, L.; Piccinelli, F.; Bettinelli, M.; Parker, S. F.; Karlsson, M. The effect of cation substitution on the local coordination of protons in $Ba_2In_{1.85}M_{0.15}O_6H_2$ (M = In, Ga, Sc and Y). *Solid State Ionics* **2021**, *365*, No. 115624.

(14) Perrichon, A.; Koza, M. M.; Evenson, Z.; Frick, B.; Demmel, F.; Fouquet, P.; Karlsson, M. Proton Diffusion Mechanism in Hydrated Barium Indate Oxides. *Chem. Mater.* **2023**, *35*, 6713−6725.

(15) Ta, T. Q.; Tsuji, T.; Yamamura, Y. Thermal and electrical properties of $Ba_2In_2O_5$ substituted for In-site by rare earth elements. *J. Alloys Compd.* **2006**, *408−412*, 253−256.

(16) Mamontov, E.; Herwig, K. W. A time-of-flight backscattering spectrometer at the Spallation Neutron Source. *Rev. Sci. Instrum.* **2011**, *82*, No. 085109.

(17) Arnold, O.; Bilheux, J.; Borreguero, J.; et al. Mantid—Data analysis and visualization package for neutron scattering and μ SR experiments. *Nucl. Instrum. Methods Phys. Res., Sect. A* **2014**, *764*, 156−166.

(18) Noferini, D.; Koza, M. M.; Karlsson, M. Localized Proton Motions in Acceptor-Doped Barium Zirconates. *J. Phys. Chem. C* **2017**, *121*, 7088−7093.

(19) Noferini, D.; Koza, M. M.; Rahman, S. M. H.; Evenson, Z.; Nilsen, G. J.; Eriksson, S.; Wildes, A. R.; Karlsson, M. Role of the doping level in localized proton motions in acceptor-doped barium zirconate proton conductors. *Phys. Chem. Chem. Phys.* **2018**, *20*, 13697−13704.

(20) Karlsson, M.; Matic, A.; Engberg, D.; Björketun, M. E.; Koza, M. M.; Ahmed, I.; Wahnström, G.; Berastegui, P.; Börjesson, L.; Eriksson, S. G. Quasielastic neutron scattering of hydrated $BaZr_{0.90}A_{0.10}O_{2.95}$ (A = Y and Sc). *Solid State Ionics* **2009**, *180*, 22.

(21) Naumovska, E.; Orstadius, J.; Perrichon, A.; Lavén, R.; Koza, M. M.; Evenson, Z.; Karlsson, M. Localized Proton Motions in the Proton-Conducting Perovskites $BaZr_{1−x}Sc_xO_3H_x$ (x = 0.10 and 0.50) Investigated with Quasielastic Neutron Scattering. *J. Phys. Chem. C* **2023**, *127*, 24532−24541.

(22) Hempehnann, R.; Karmonik, C.; Matzke, T.; Cappadonia, M.; Stimming, U.; Springer, T.; Adams, M. A. Quasielastic neutron scattering study of proton diffusion in $SrCe_{0.95}Yb_{0.05}H_{0.02}O_{2.985}$. *Solid State Ionics* **1995**, *77*, 152−156.

(23) Karlsson, M. Proton dynamics in oxides: insight into the mechanics of proton conduction from quasielastic neutron scattering. *Phys. Chem. Chem. Phys.* **2015**, *17*, 26−38.

(24) Noferini, D.; Koza, M. M.; Fouquet, P.; Nilsen, G. J.; Kemei, M. C.; Rahman, S. M.; Maccarini, M.; Eriksson, S.; Karlsson, M. Proton Dynamics in Hydrated $BaZr_{0.9}M_{0.1}O_{2.95}$ (M = Y and Sc) Investigated with Neutron Spin-Echo. *J. Phys. Chem. C* **2016**, *120*, 13963−13969.

(25) Yamazaki, Y.; Babilo, P.; Haile, S. M. Defect Chemistry of Yttrium-Doped Barium Zirconate: A Thermodynamic Analysis of Water Uptake. *Chem. Mater.* **2008**, *20*, 6352−6357.

(26) Mazzei, L.; Perrichon, A.; Mancini, A.; Wahnström, G.; Malavasi, L.; Parker, S. F.; Börjesson, L.; Karlsson, M. Local structure and vibrational dynamics in indium-doped barium zirconate. *J. Mater. Chem. A* **2019**, *7*, 7360−7372.

(27) Chudley, C. T.; Elliott, R. Neutron Scattering from a Liquid on a Jump Diffusion Model. *Proc. Phys. Soc.* **1961**, *77*, 353.

(28) Lohstroh, W.; Zachary, E. TOFTOF: Cold neutron time-of-flight spectrometer. *J. Large Scale Res. Facil.* **2015**, *1*, A15.